Energy & Environmental Science

Cite this: *Energy Environ. Sci.*, 2011, **4**, 1621

www.rsc.org/ees

PERSPECTIVE

Who will drive electric vehicles, olivine or spinel?

Ok Kyung Park, Yonghyun Cho, Sanghan Lee, Ho-Chun Yoo, Hyun-Kon Song* and Jaephil Cho*

Received 13th October 2010, Accepted 4th January 2011
DOI: 10.1039/c0ee00559b

Lithium iron phosphate olivine (LFP) and lithium manganese oxide spinel (LMO) are competitive and complementary to each other as cathode materials for lithium ion batteries, especially for use in hybrid electric vehicles and electric vehicles. Interest in these materials, due to their low cost and high safety, has pushed research and development forward and toward high performance in terms of rate capability and capacity retention or cyclability at a high temperature of around 60 °C. From the view point of basic properties, LFP shows a higher gravimetric capacity while LMO has better conductivities, both electrically and ionically. According to our comparison experiments, depending on the material properties and operational potential window, LFP was favored for fast charging while LMO led to better discharge performances. Capacity fading at high temperatures due to metal dissolution was revealed to be the most problematic issue of LFP and LMO-based cells for electric vehicles (EVs), with thicker electrodes, in the case of no additives in the electrolyte and no coating to prevent metal dissolution on cathode materials. Various strategies to enhance the properties of LFP and LMO are ready for the realization of EVs in the near future.

1. Introduction

Rechargeable batteries based on lithium ions are considered as the most dominant technology in the field of energy storage due to their high energy density. Since lithium ion batteries (LIBs) were introduced into market, the application targets have evolved from small mobile devices such as camcorders, cell phones, digital cameras and laptop computers, to large-scale applications including hybrid electric vehicles (HEVs), electric vehicles (EVs) and stationary energy storage wells.

Obviously, much concern is devoted to HEV or EV applications of LIBs. It must be one of the main issues to choose cathode materials in terms of energy density, power density (rate capability), cycle life (stability), safety and cost (material and process costs). Lithium manganese oxide with a spinel structure (LMO spinel, $LiMn_2O_4$) and lithium iron phosphate with an olivine structure (LFP olivine, $LiFePO_4$) are being competitively developed for the target fields. The main stream of cathode materials is LMO spinel from Korea and Japan, and LFP olivine from China and the USA.

The dominant factor of these materials is low price and good safety, compared with conventional cathode materials popularly used in portable electronics applications (*e.g.* $LiCoO_2$). LMO spinel and LFP olivine have their own merits relative to their counterparts when compared with one another (Table 1).

We believe that it is time to review those strongest candidates as cathode materials for electric vehicles. Merits and demerits of their intrinsic properties will be compared bibliographically and experimentally, and then ways to overcome the demerits will be discussed based on a survey of technical literature. It will be concluded with what will be a practical solution or direction for the immediate future.

i-School of Green Energy, UNIST (Ulsan National Institute of Science & Technology), Ulju, Ulsan, 689-798, Korea. E-mail: philiphobi@unist.ac.kr; jpcho@unist.ac.kr

Broader context

Recently, applications of the lithium ion batteries (LIBs) have extended to hybrid electric vehicles (HEVs), and electric vehicles (EVs), and one of the main issues for such applications is to enhance the performances of cathode materials in terms of energy density, power density (rate capability), cycle life (stability), safety and cost (material and process costs). Lithium manganese oxide with a spinel structure (LMO spinel, $LiMn_2O_4$) and lithium iron phosphate with an olivine structure (LFP olivine, $LiFePO_4$) are being competitively developed for the target fields. Interest in these materials, due to their low cost and high safety, has pushed research and development forward and toward high performance in terms of rate capability and capacity retention or cyclability at a high temperature of around 60 °C.

Table 1 Intrinsic material properties of LMO spinel *versus* LFP olivine[a]

	LMO spinel $LiMn_2O_4$	LFP olivine $LiFePO_4$
Working potential (V *vs.* Li/Li^+)	4.0–4.2 (Up to 80% Li^+ use) 3.0 (Additional Li^+ use, practically meaningless)	3.45
Capacity at low C rates (<0.1 C) (mA h g^{-1})	148 (Theoretical) 100–130 (Practical)	170 (Theoretical) 150 (Practical)
Energy density (W h kg^{-1})	607 (Theoretical) 410–530 (Practical)	590 (Theoretical) 520 (Practical)
Electrical conductivity[1] (S cm^{-1})	10^{-4}	$10^{-9\text{ to }-8}$
Ionic conductivity[1–3] (S cm^{-1})	10^{-6}	$10^{-11\text{ to }-9}$
Ionic diffusivity[4–7] (cm^2 sec^{-1})	$10^{-11\text{ to }-9}$	$10^{-17\text{ to }-12}$ $10^{-8\text{ to }-7}$ (calculated)
Cost ($ kg^{-1})	10–15 Low	20–25 Possibly low, but limited by patent issues and process cost[b]

[a] Properties related to electronic and ionic transport are the values at room temperature. [b] More sophisticated synthesis techniques are required, including preparation of nano-sized materials to overcome low conductivities and protecting oxidation of Fe^{2+} during thermal treatment.

2. Material properties

2.1 Basic properties

$LiMn_2O_4$ spinels are promising materials for medium and large size Li-ion batteries as power sources of HEVs or EVs, and have been extensively studied and commercially used because of lower costs, high rate capability and higher thermal stability compared to $LiCoO_2$ and $LiNi_{1-x}M_xO_2$ materials.[8–12] However, the main problem for the application of spinel materials is capacity fading at elevated temperatures, above 60 °C,[13–17] which is due to Mn dissolution *via* the disproportion reaction proposed by Hunt *et al.*:[18] $2Mn^{3+} \rightarrow Mn^{2+} + Mn^{4+}$.

In the ideal spinel $LiMn_2O_4$ structure, oxygen atoms form a face-centered cubic packing structure and occupy 32e sites of the space group of Fd3m (Fig. 1a). The Li atoms are located in the tetragonal 8a sites, while the Mn atoms occupy the octahedral 16d sites, and the octahedral 16c sites remain empty. The 8a and 16c sites form a three-dimensional pathway for lithium diffusion. When the lithium mole fraction exceeds 1 ($Li_{1+x}Mn_{1-y}O_4$), the lithium ions enter the vacant 16c sites.

Another type of spinel is 5 V $LiNi_{1.5}Mn_{0.5}O_4$. In order to improve its structural instability, substitution of transition metals (M = transition metal) into the Mn sites in $LiM_xMn_{2-x}O_4$ has been investigated intensively.[19–22] Among the transition metals, $LiNi_{0.5}Mn_{1.5}O_4$ spinel exhibited an additional ~4.7 V plateau due to the presence of a Ni^{2+}/Ni^{4+} redox pair, thus delivering >100 mA h g^{-1} reversible capacity. However, due to its high operation voltage, the electrolyte is easily oxidized, therefore much more work should be accomplished before its use in EVs. Therefore, in this review, 5 V spinels are not discussed any further.

For $LiFePO_4$, the olivine compound consists of distorted FeO_6, LiO_6, and PO_4 units (Fig. 1b), and there is no continuous network of edge-sharing FeO_6 octahedra to reduce the electronic conductivity, which is polaronic in the mixed-valence state. The electrochemical charge/discharge potential profile is very flat and located at 3.45 V *vs.* Li/Li^+, and its theoretical capacity is relatively high (170 mA h g^{-1}) compared to $LiMn_2O_4$ spinel (148 mA h g^{-1}). However, one of the main problems of the $LiFePO_4$ olivine is the low electronic conductivity. The electrical

Hyun-Kon Song

Prof. Hyun-Kon Song is in the Interdisciplinary School of Green Energy from UNIST (Ulsan National Institute of Science and Technology), Korea. He received his Ph. D. in Chemical Engineering from POSTECH, Korea. He has been a postdoctoral researcher at Brown University and Seoul National University, and a senior researcher at LG Chem/ Research Park. His research disciplines are based on electrochemistry and bioinspired chemistry for energy, covering synthesis of electroactive materials and novel design of electrochemistry-based devices.

Jaephil Cho

Jaephil Cho is a professor and dean in the Interdisciplinary School of Green Energy at UNIST, Korea. He received his Ph. D. in Ceramic Engineering from Iowa State University, USA, in 1995. He is a director of the Converging Research Center for Innovative Battery Technologies supported by the Ministry of Education, Science & Technology in Korea. His current research is focused mainly on nanomaterials for energy conversion and storage, nanoscale coating, and safety enhancement of Li-ion batteries and Metal-Air cells.

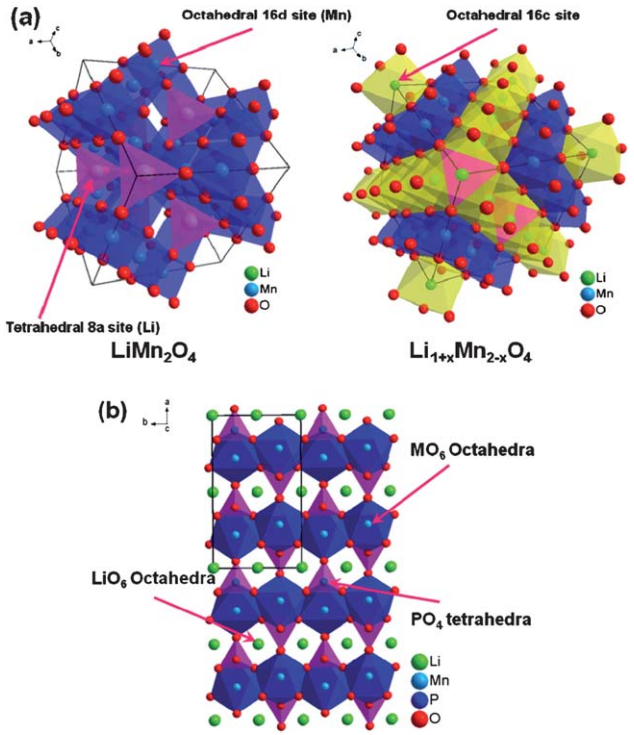

Fig. 1 Crystal structure of (a) $LiMn_2O_4$ (LMO), (b) $Li_{1+x}Mn_{2-x}O_4$ and (c) $LiFePO_4$ (LFP).

conductivity and lithium ion diffusivity are two of the most important properties responsible for the electrochemical performance of the battery cathode. Low conductivity may lead to a poor rate capability because it provides a kinetic limitation and induces polarization during the lithium intercalation and deintercalation.

Fig. 2 shows some SEM images of the $LiFePO_4$ (carbon content 2 wt%) and $Li_{1.1}Mn_{1.91}Al_{0.09}O_4$ spinel particles. LFP particles consist of dispersed nanoparticles of approximately 100 nm diameter, and an inset confirms the formation of a turbostatic carbon coating layer with a thickness of 4 nm. On the other hand, LMO consists of spherical particles with an average particles size of ~15–20 μm, in which each particle consists of octahedral primary particles with sizes of 1–3 μm. Powder XRD patterns of both particles show the formation of pure olivine and spinel phases without any impurities (Fig. 3).

During storage, delivery and processing, the active materials are exposed to air and moisture, and the water contents of as-prepared LMO and LFP were 70 and 100 ppm, respectively. To minimize the air-exposure, both samples were kept in a dry-box. In particular, the Fe^{2+} ions in LFP are easily corroded (oxidized) in presence of oxygen and water in air, therefore carbon coating was essential. Slurry preparation and the electrode coating processes of those materials were done under a relative humidity of <30%.

2.2 Mn^{3+} dissolution of LMO

Two possible Mn^{3+} dissolution mechanisms have been proposed (Fig. 4). One suggests that surface water molecules (Mn–OH)

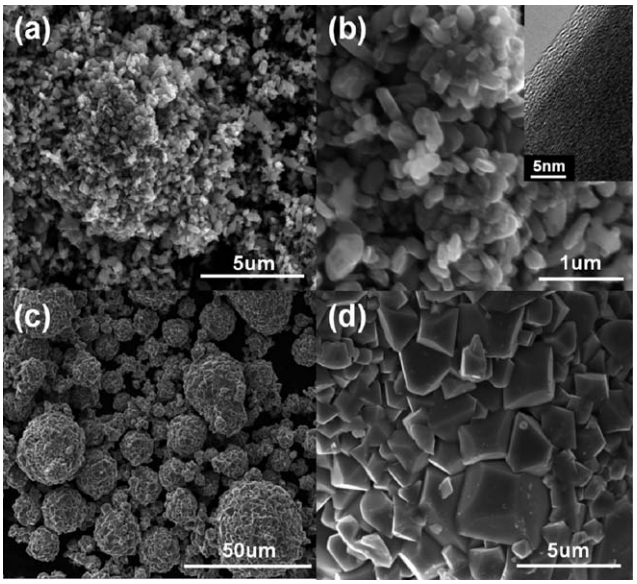

Fig. 2 SEM images of the $LiFePO_4$ (carbon content 2 wt%) and $Li_{1.1}Mn_{1.91}Al_{0.09}O_4$ spinel particles.

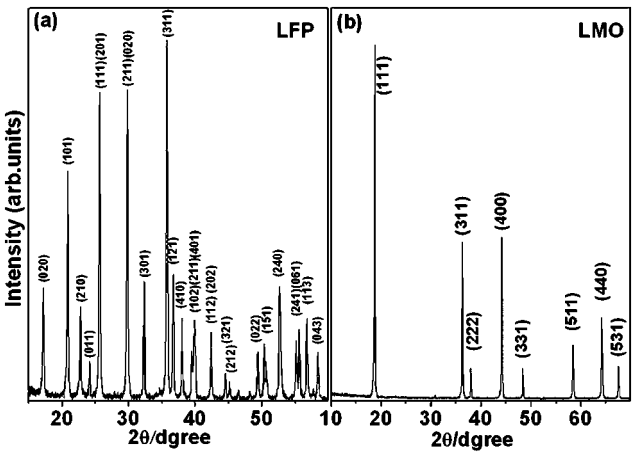

Fig. 3 Powder XRD patterns of $LiFePO_4$ (carbon content 2 wt%) and $Li_{1.1}Mn_{1.91}Al_{0.09}O_4$ spinel particles.

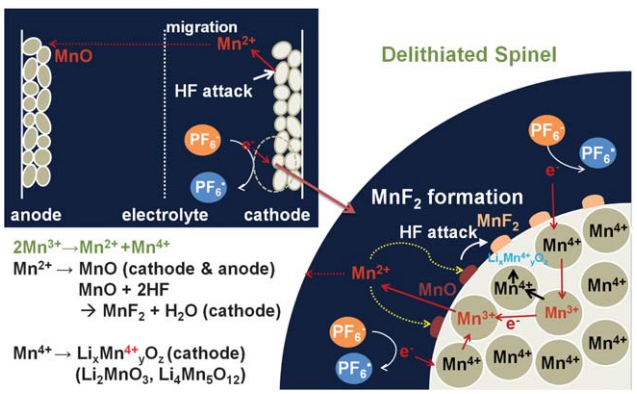

Fig. 4 Mechanisms of Mn^{3+} dissolution.

react with $LiPF_6$ by a cation exchange reaction and HF molecules are formed according to a series of reactions:[16,23]

$$LiPF_6 \leftrightarrow LiF(s) + PF_5$$

$$PF_5 + H_2O \leftrightarrow POF_3 + 2HF$$

$$POF_3 + H_2O \leftrightarrow PO_2F_2H + HF$$

$$PO_2F_2H + H_2O \leftrightarrow PO_3FH_2 + HF$$

$$PO_3FH_2 + H_2O \leftrightarrow PO_4H_3 + HF$$

Here, H^+ ions in HF produce MnO and MnO_2 according to $2LiMn_2O_4 + 4H^+ \rightarrow 3MnO_2 + MnO + Li_2O + 2H_2O$.[24] Also, in a similar manner, since the HF environment is corrosive, MnF_2 formation is possible according to the following reaction:[25]

$$2LiMn_2O_4 + 4H^+ + 4F^- \rightarrow 3MnO_2 + MnF_2 + 2LiF + 2H_2O$$

However, in charged states at an elevated temperature, PF_6^- ions are apt to reduce to PF_5^-, and therefore Mn^{4+} ions are more apt to reduce to Mn^{3+}, as follows:

$$LiPF_6 \rightarrow PF_5 + e^-$$

$$Mn^{4+} + e^- \rightarrow Mn^{3+}$$

This is why Mn dissolution is accelerated at elevated temperatures, whilst simultaneously spinel turns into defective spinels with Mn^{4+} (Li_2MnO_3 and $Li_4Mn_5O_{12}$).[24,26]

The possible formation of MnF_2 was observed by Quinlan *et al.*[27] X-Ray photoelectron spectroscopy of the $Li_xMn_2O_4$ particles after storage at 70 °C for 2 days showed the MnF_2 peak at 684.6 eV, but its peak is overlapped with LiF peak. Fig. 5 shows TOF-SIMS (Time of Flight Secondary Ion Mass Spectrometry) spectra of EV-LMO electrodes before and after 100 cycles at 60 °C, and an MnF^+ peak is clearly observed at ~79 m/Z, which is the first evidence for the formation of MnF_2 on the particle surface.

2.3 Instability of LFP at high temperatures

One of the reasons that LFP olivine is a promising cathode material is its thermal stability. The thermal stability of LFP (not in cells but the material itself) will be shown in the following section, which is proven by the lack of clear exothermal peaks and distinguishable structural change, at least up to 500 °C. However, the thermal stability of LFP in an electrolyte, even under applied potential during charge/discharge processes, cannot be guaranteed by the thermal stability of materials.

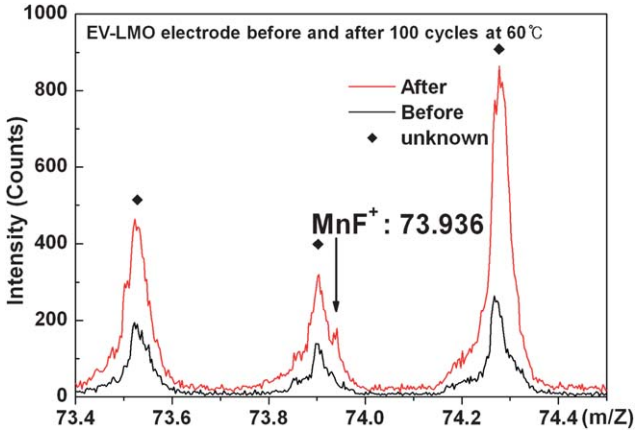

Fig. 5 TOF-SIMS spectra of EV-LMO electrodes before and after 100 cycles at 60 °C.

Iltchev *et al.* compared LFP with LMO in terms of their solubility in an electrolyte (1 M $LiPF_6$ in EC : DMC (1 : 1)) at room temperature, 65 °C and 80 °C.[28] Results suggested that the thermal stability of LFP is superior to that of LMO in the case of no applied potential. No evidence of significant Fe dissolution was found at any temperature, independent of storage time (up to 4 days), while very significant amounts of Mn in the electrolyte were detected at 60 °C (100 ppm) and at 85 °C (450 ppm) after 4 days of storage.

Contradicting results on the solubilization were reported by Koltypin *et al.*, which supported the feasibility of Fe dissolution in an electrolyte: 40% of atomic iron was dissolved from LFP at 60 °C after 20 days of storage in the same electrolyte as used by Iltchev *et al.*[29] Fe was not found in the electrolyte at room temperature. For an exact comparison, 8% loss is expected after 4 days of storage. Amine *et al.* also reported that metal dissolution is more serious in LFP at 55 °C than in LMO: ~600 ppm Fe^{2+} dissolution from non-coated or carbon-coated LFP after a week of aging in 1.2 M $LiPF_6$ in EC : EMC (3 : 7) *versus* 64 ppm from LMO after four weeks of aging in 1.2 M $LiPF_6$ in EC : DEC (1 : 1).[30,31]

Various electrolytes have been tested in the presence of additives.[29] The most serious Fe dissolution was observed in the same electrolyte with 100 ppm H_2O. It is well known that HF forms *via* the unwanted reaction between $LiPF_6$ and a trace of water (reactions shown in Section 2.2). Fe dissolution is initiated by the mechanism of ion exchange between acidic protons and iron ions ($2H^+ \leftrightarrow Fe^{2+}$). By adding an acid scavenger such as Li_2CO_3, the problem is overcome: $Li_2CO_3 + 2HF \leftrightarrow 2LiF + H_2CO_3$. Also, the use of non-fluorinated salts such as $LiClO_4$,[29] and $LiB(C_2O_4)_2$,[30] is helpful to suppress the metal dissolution.

Amine *et al.* investigated capacity fading of LFP-based cells at 55 °C.[30] They reported the change of discharge capacity with cycles for three different cells. The first cell (carbon-coated LFP with Li metal as an anode in an unknown electrolyte) showed very good cyclability up to 100 cycles. However, the other two cells (non-coated or carbon-coated LFP with MCMB carbon in 1.2 M $LiPF_6$ in EC : EMC (3 : 7)) showed serious capacity fading to 70% loss at the 100th cycle (ΔQ_{100} (graphite, 55 °C, 1.2 M, 3 : 7 EC : EMC) = 70%). Even if the reason for the good cyclability of

the first cell was not discussed, the work concluded that Fe dissolution can cause serious capacity fading. Fe dissolution-induced capacity fading was confirmed in other works: ΔQ_{100} (graphite, 55 °C, 1 M, 1 : 2 EC : MEC) = 25%;[32] ΔQ_{200} (Li, 55 °C, 1 M, 1 : 2 EC : MEC) = 20%;[32] ΔQ_{100} (graphite, 60 °C, 1 M, 1 : 1 EC : DEC) = 50%.[33]

The increase of impedance and the decrease of capacity with cycles at high temperature (usually tested at 55 °C or 60 °C) originate from Fe dissolution, causing the following changes:

(i) The structure of a portion of LFP is changed from olivine to an amorphous phase with the loss of Fe^{2+}.[29]

(ii) A passive layer is formed on the surface of LFP by the reaction between HF and LFP.[29,32] The surface layer consists of inorganic compounds such as LiF, Li_xPF_y and $LiPO_yF_z$, and organic species such as carbonyl-containing surface compounds. LiF film is highly resistant to Li^+ migration.

(iii) Anodes are passivated by a thick solid–electrolyte interphase (SEI) layer that is formed catalytically by Fe metal deposited on the anodes.[30,32]

In addition to the use of inorganic additives (Li_2CO_3) or the replacement of $LiPF_6$ with other salts as mentioned above, a more practical solution to overcome the Fe dissolution has been proposed. Vinylene carbonate (VC), the popular solid–electrolyte interphase layer forming agent for graphite anodes, was used as an organic additive in the electrolyte to suppress metal dissolution.[32] Minor capacity loss was investigated compared with its without-VC counterpart: ΔQ_{1000} (graphite, 55 °C, 1 M, 1 : 2 EC : MEC) = 20%;[32] ΔQ_{200} (Li, 55 °C, 1 M, 1 : 2 EC : MEC) = 20%.[32] The use of VC prohibited the formation of Fe dissolution-related layers on cathodes and anodes. While the use of VC is a solution on the electrolyte side, AlF_3 coating on LFP particles is the electrode solution. The inorganic coating led to a capacity loss from 50% for bare LFP to less than 10%.[33]

Even if several research works have been devoted to solving the problem of Fe dissolution by additional endeavours, Zaghib *et al.* showed very good capacity retention over only 200 cycles by using synthetically optimized carbon-coated LFP. The mixture of $FePO_4(H_2O)_2$ and Li_2CO_3 was heated at 700 °C for 8 h to obtain the olivine phase. The LFP was thermally treated again with a carbon precursor (sucrose or cellulose acetate) under the same conditions.

2.4 Thermal stability of LMO and LFP

Fig. 6 shows some differential scanning calorimeter (DSC) scans of $Li_{0.05}FePO_4$ between 50 and 500 °C at a scan rate of 10 °C min^{-1} (for reference, blank empty pans were also run). These cathode materials were also compared with the $Li_{0.2}Ni_{0.7}Mn_{0.15}Co_{0.15}O_2$, in which a very sharp exothermic peak at 234 °C is indicative of sudden oxygen release from the cathode as a result of decomposition from a layered to a spinel phase. Note that the onset temperature of $Li_{0.2}Ni_{0.7}Mn_{0.15}Co_{0.15}O_2$ is 223 °C, which is a starting temperature of oxygen evolution from the lattice. Such an abrupt peak leads to an incident thermal runaway that should be avoided in a Li-ion battery. On the other hand, LFP shows a negligible exothermic peak at 374 °C, which means there is little oxygen evolution from the lattice. Similar to this behavior, LMO cathodes show minor peaks between 250 °C and 300 °C (three test cells showed same trends).

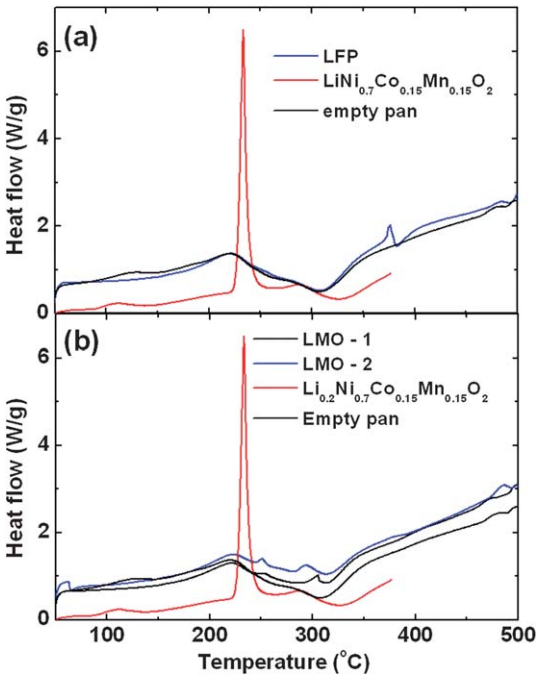

Fig. 6 DSC scans of (a) $Li_{0.05}FePO_4$ and (b) $Li_{0.05}Mn_2O_4$ cathodes between 50 °C and 500 °C at rate of 10 °C min^{-1}. All the electrodes were soaked with the electrolytes.

In order to investigate the structural stability of the delithiated LFP and LMO electrodes, *in situ* XRD patterns of both samples were investigated, as shown Fig. 7. LFPs did not show any new formation of secondary peaks as a result of oxygen evolution from the lattice, but the diffraction peaks started to diffuse a little with increasing temperature. Although there are many origins for such behavior, we suspect the formation of a disordered oxygen deficient $FePO_{4-\delta}$ phase. On the other hand, $Li_{0.05}Mn_2O_4$ showed dominant λ-MnO_2 peaks up to 200 °C, and turned into β-MnO_2 at 250 °C. However, the β-MnO_2 peaks were diffused, which is indicative of disordered oxygen deficient phase formation since the results from DSC also exhibited minor peaks between 250 °C and 300 °C. There were no more peak changes observed up to 500 °C.

3. Experimental comparison

3.1 Cell preparation

LIB cells were prepared considering two different types of vehicles driven by electricity: HEVs and EVs. Rechargeable batteries used in HEVs are charged by an electric generator driven by the internal combustion engine during a regenerative braking mode. The electric energy is used to assist horsepower of the engine during drive mode. Power density rather than energy density is the main concern of the cells for HEVs because fast charge and discharge is required for this *in situ* energy transfer. In contrast, the cells for EVs should be developed to have high energy density. The rechargeable batteries are a sole energy source for EVs, which indicates that the energy density of batteries for EVs should be comparative with that of fuels for internal combustion engines such as gasoline. Therefore, cells for EVs were designed to have double the capacity of those for HEVs (Table 2). With

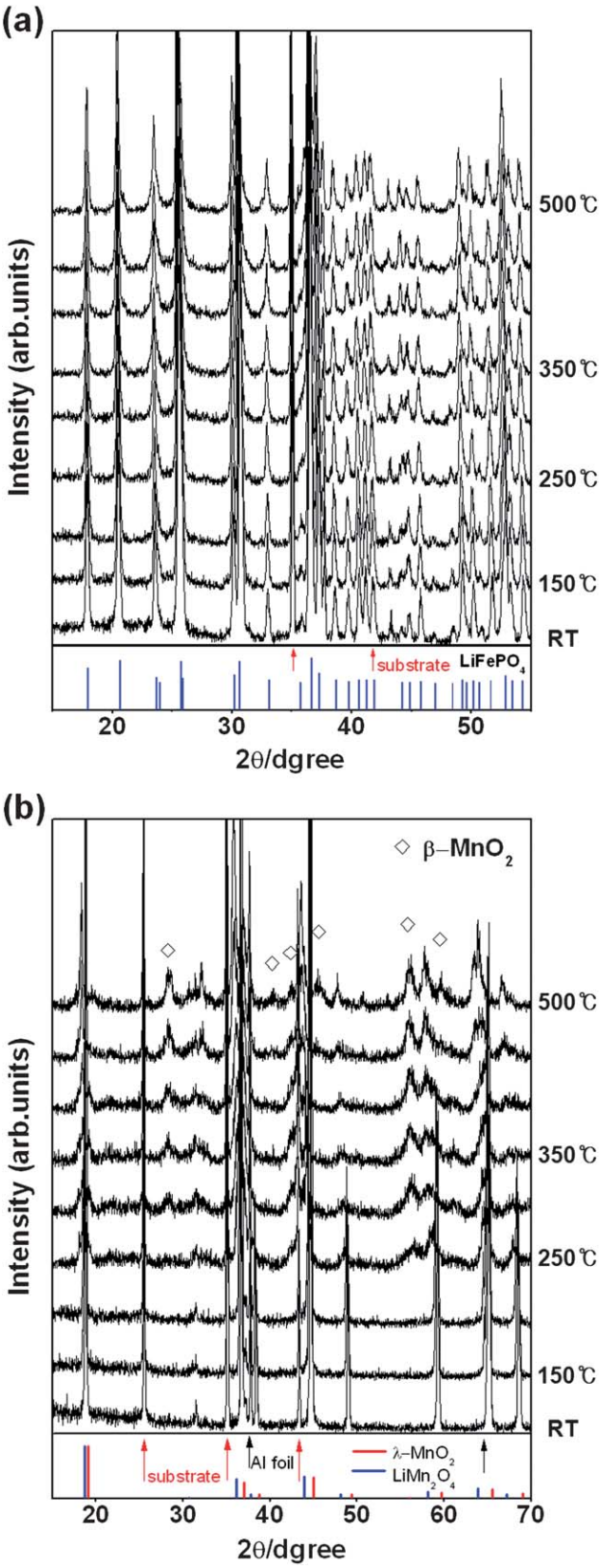

Fig. 7 *In situ* XRD patterns of (a) $Li_{0.05}FePO_4$ and (b) $Li_{0.05}Mn_2O_4$ electrodes at a scan rate of 50 °C.

Table 2 Specification of electrodes of LIBs for HEVs and EVs

	LMO		LFP	
	HEV	EV	HEV	EV
Areal capacity (mA h cm^{-2})	1	2	1	2
Thickness (μm) (except for Al foil)	50	100	50	100
Density of active materials in electrode paste (g cm^{-3})	1.7		1.3	
Composition (wt%) Active : Super-P : PVdF	80 : 10 : 10		92 : 4 : 4	

a fixed density, the electrode paste (consisting of an active material, a conductive material and a binder) for HEVs was twice as thick as that for HEVs.

LMO or LFP was used as the active cathode material while carbon black (Super-P) and PVdF were used as the conductive agent and the binder, respectively. Commercially available products were used as the active materials of LMO and LFP. LMO was doped with aluminium ($Li_{1.1}Mn_{1.91}Al_{0.09}O_4$) while LFP was coated with carbon at 2 wt%. Larger amounts of carbon black, and subsequently larger amounts of PVdF were used for LFP due to its lower conductivity. An additive-free electrolyte (1.15 M $LiPF_6$ in 3 : 4 : 3 vol. % ethylene EC DMC DEC, where EC = ethylene carbonate, DMC = dimethyl carbonate, DEC = diethyl carbonate) was used in a half coin cell configuration with lithium metal as a reference electrode to investigate the genuine properties of the active materials. 20 μm-thick microporous polyethylene film (Tonen E20MMS) was used as a separator between the cathode and lithium metal.

3.2 Capacities at various discharge rates

Discharge capacity depends on discharge rate, the materials used, and the thickness of electrodes. Dependency of discharge capacities on discharge rates were compared between LMO and LFP for HEV and EV cells (Fig. 8). The cells were charged galvanostatically to 4.3 V at 0.1 C. After 4.3 V was reached, their

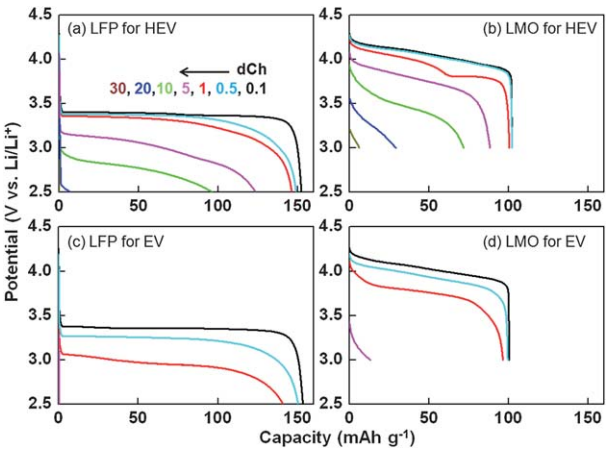

Fig. 8 Discharge profiles of potential *versus* capacity with various discharge rates. The cells were charged galvanostatically to 4.3 V at 0.1 C. After 4.3 V was reached, their potential was kept at 4.3 V until the current had decreased to a hundredth of its initial value. Cells were run at 21 °C.

potential was kept at 4.3 V until the current had decreased to a hundredth of its initial value. Then, the cells were discharged at various rates to 2.5 V for LFP and 3.0 V for LMO. The operational potential window (ΔE_{op}) was set wider for LFP (ΔE_{op}(LFP) = 4.3 V − 2.5 V = 1.8 V) compared with LMO (ΔE_{op}(LMO) = 4.3 V − 3.0 V = 1.3 V) because the electrochemical potential of LFP (3.45 V) is much lower than that of LMO (~4.1 V). With the end potentials for discharge, the working potential window available for extracting energy (ΔE_w^{dCh}) is similar between the cathode materials: ΔE_w^{dCh}(LFP) = 3.45 V − 2.5 V = 0.95 V and ΔE_w^{dCh}(LMO) = 4.1 V − 3.0 V = 1.1 V.

For the thinner electrodes of the HEV cells, about 70% of the capacity at 0.1 C (Q_m^{dCh} (0.1 C)) was obtained at 10 C for both LMO and LFP in a similar working potential window. However, the lower resistance of the LMO electrode (originating from higher conductivity of LMO compared to LFP) is expected from the values of *IR* drop (ΔIR) occurring just after the start of discharge. At 10 C, for example, ΔIR(LFP) = 3.45 V − 3.0 V = 0.45 V while ΔIR(LMO) = 4.1 V − 3.9 V = 0.2 V. As the discharge rate increases, the effect of ΔIR becomes more serious and the difference between cathode materials can be seen: the discharge capacity was not available at 20 C for LFP while 30% of Q_m^{dCh} (0.1 C) was obtained at the same C rate for LMO.

It is natural that rate capability becomes worse with thicker electrodes: EV cells did not provide an available capacity at 10 C for both LFP and LMO. LMO still showed a slightly better rate capability with smaller *IR* drop: at 1 C, for example, capacity = 91% of $Q^{dCh}{}_{0.1C}$ with ΔIR = 0.45 V for LFP *versus* 95% with ΔIR = 0.25 V for LMO.

Even if the gravimetric capacity (Q_m^{dCh}, mA h g^{-1}) of LFP is larger than that of LMO, the order relation between LFP and LMO is changed in terms of volumetric energy density (ED_v^{dCh} mW h cm^{-3}). Two factors should be considered: working potential and electrode density. LMO shows a slightly inclined plateau at a fairly high potential (4.1 V) compared with the working potential of LFP at 3.45 V. The higher potential leads to the increase of energy density. Also, since a larger amount of LMO was used to build the electrodes (92 wt% LMO *versus* 80 wt% LFP), the electrodes based on LMO are denser than those based on LFP in terms of the density of active materials in the electrode paste (Table 2). As a result, the volumetric capacity shows the order relation between LMO and LFP to be quite different from the gravimetric capacity. That is to say, the cells based on LMO have a higher volumetric energy density compared with their counterparts: at 0.1 C, for example, ED_v^{dCh} = 700 mW h cm^{-3} for LMO *versus* 665 mW h cm^{-3} for LFP.

Capacity recovery was good for both cathode materials independent of their applications (Fig. 9). An almost 100% recovery of capacity at 0.1 C was obtained after a series of fast discharges consisting of 3 cycles at 0.1 C and 10 cycles at 10 C and 50 C. This result indicates that there is no damage to the electrodes.

3.3 Capacities at various charge rates

Charge rate is another important operational variable that should be considered, especially in HEV/EV applications. Dependency of discharge capacity on charge rate determines how efficiently batteries are charged without any loss during the regenerative braking mode of HEVs, and how long it takes for the charging of EVs. In small scale appliances such as cellular phones and laptop computers, this operational variable is not the main concern.

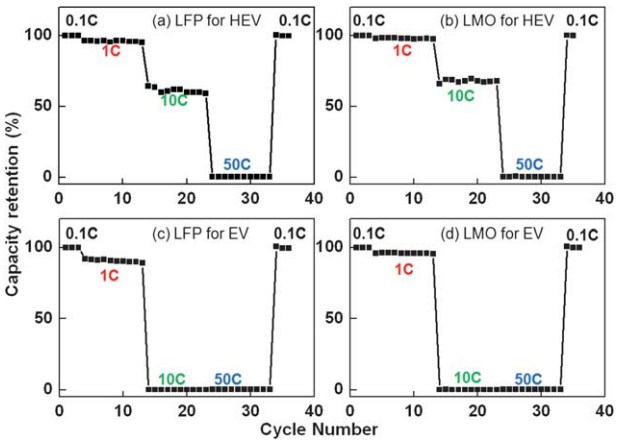

Fig. 9 Discharge capacities at various discharge rates. The same conditions were used as indicated in Fig. 8.

Dependency of discharge capacity on charge rate was compared between LMO and LFP for HEV and EV cells (Fig. 10). The cells were charged to 4.3 V at various charge rates without following a constant voltage mode. The reason for using only the constant current mode is to investigate the effect of charge rate, which determines charge time. It would be meaningless in terms of charge time to charge cells fast at high current and then to keep potential for long time. The charged cells were discharged at a low C rate (0.1 C) to 2.5 V for LFP and 3.0 V for LMO. The amount of charged energy was fully extracted without any loss because cells were discharged slowly enough.

For the thinner electrodes of the HEV cells, LFP-based cells showed better charge rate capability than their counterpart: 70% of the charged capacity at 0.1 C (Q_m^{Ch} (0.1 C)) was charged at 10 C for LFP while the potential reached 4.3 V after charging at 10 C in the case of LMO. For the thicker electrodes of the EV cells, also, better charge rate capability was observed with LFP.

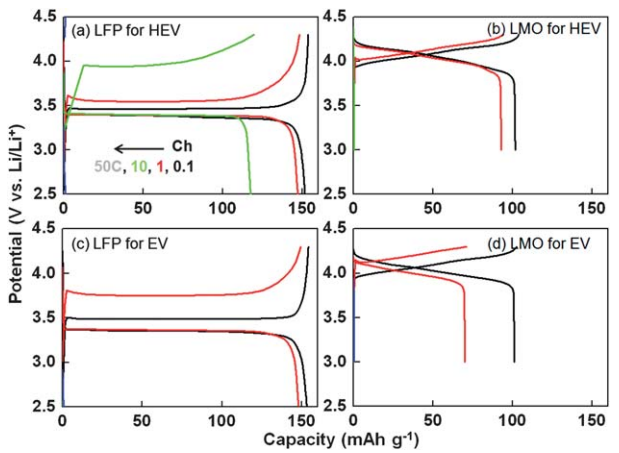

Fig. 10 Charge profiles and the corresponding discharge profiles of potential *versus* capacity with various charge rates. Cells were charged to 4.3 V at various charge rates without following constant voltage mode. Charged cells were discharged at 0.1 C.

Even if Fig. 10 indicates LFP is superior to LMO in terms of capacity at a high charge rate, the better performance of LFP over LMO does not originate from the intrinsic material properties. Rather, electric conductivity and ionic diffusivity of LMO is higher than those of LFP. The reason should be sought in the operational conditions. The charging potential was set at 4.3 V for both LFP and LMO. The working potential window available for storing energy (ΔE_w^{Ch}) is much narrower for LMO (ΔE_w^{Ch}(LMO) = 4.3 V − 4.0 V = 0.3 V) compared with LFP (ΔE_w^{Ch}(LFP) = 4.3 V − 3.45 V = 0.85 V). Therefore, even if the potential change due to *IR* drop (actually, *IR* rise) occurring just after the start of charge was smaller for LMO than that for LFP, the potential margin is too small to store energy in the case of LMO compared with LFP. Compared with LFP, therefore, LMO shows inferior charge rate capability due to the restricted potential window for charge even if it shows better discharge rate capability due to its higher conductivity.

A different composition of electrodes was used for LFP (80%) and LMO (92%) as the conductivity of LMO is superior to that of LFP. To compare the cathode materials under identical conditions, the same composition (80%) was tested for LMO (Fig. 11). In variable discharge rate experiments, a subtle enhancement of rate capability was observed in (a), compared with the 92% composition shown in Fig. 8b. This indicates that the amount of conductive materials (4%) in the 92% composition would be enough to make a conductive percolation network over the electrodes, at least in terms of discharge. On the other hand, enhanced rate capability was observed in the variable charge rate experiments: Q_m^{dCh} at 10 C (= 48 mA h g^{-1}) is available for the 80% composition while the 92% composition was not charged due to the *IR* rise. However, 80% LMO did not overcome the limit of the working potential window, considering Q_m^{dCh} at 10 C is still lower than that of LFP.

3.4 Stability of cells stored at 60 °C

To investigate the degree of deterioration of active materials at a high temperature (60 °C), the open circuit potential (OCV) of fully charged cells was traced for four weeks (Fig. 12). Discharge profiles of cells were checked at the same temperature every week (Fig. 13) and then the cells were restored at 60 °C after a full charge.

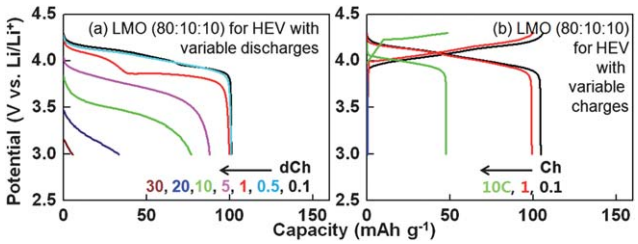

Fig. 11 Discharge/charge profiles of potential *versus* capacity of LMO for HEVs. The composition of 80 : 10 : 10 (active : Super-P : PVdF) was used for preparing electrodes. It should be noted that this composition of LMO was used only for this figure. In all other figures, 92 : 4 : 4 was used for LMO. (a) Variable discharge rate experiments. The same conditions were used as indicated in Fig. 8. (b) Variable charge rate experiments. The same condition is used as indicated in Fig. 10.

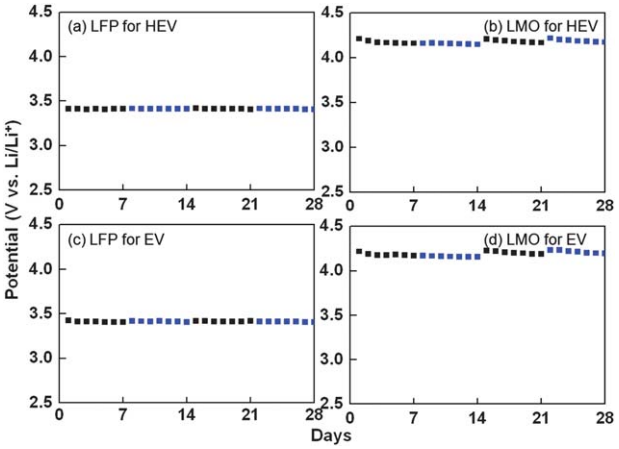

Fig. 12 Temporal change of the open circuit potential (OCV) of cells stored at 60 °C. The cells were discharged and fully charged again every week.

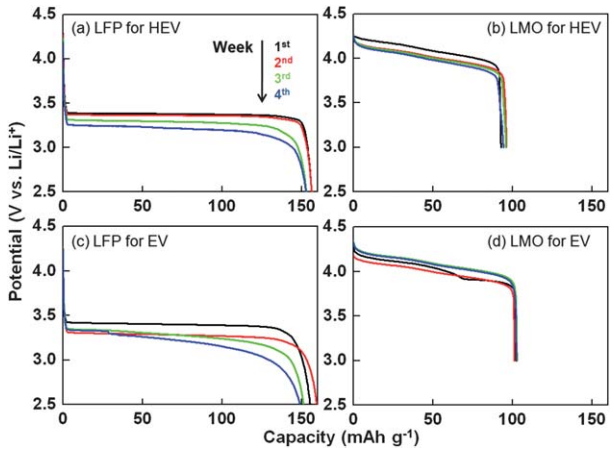

Fig. 13 Discharge profile of potential *versus* capacity of cells stored at 60 °C. The profiles were obtained at 60 °C every week. Cells were charged to 4.3 V at 0.5 C, followed by keeping the potential constant until the current decreased to a hundredth of the initial current. Then, the cells were discharged at 1 C.

Both cells based on LFP and LMO showed a stable open circuit potential at 3.45 V for LFP and 4.2 V for LMO (Fig. 12). In more detail, a perfectly flat trace was obtained with LFP within every one week period, while a slight decrease of OCV was obtained with LMO. The behaviours of the OCV reflect the nature of the reactions of the active materials. LFP is based on a two phase reaction, leading to a very flat profile (potential *versus* capacity in Fig. 8a and c) at the working potential. There would be no change of OCV even with some loss of capacity due to self discharge or material deterioration. On the other hand, LMO is based on a solid solution reaction leading to a slightly inclined plateau in its potential profile (Fig. 8b and d). The working potential is not well defined during the discharge or charge processes because the composition of LMO is changed. Therefore, even with a slight loss of capacity, potential could decrease (even if the degree of decrease is not serious).

In addition to OCV, potential profiles should be investigated to give the statement of no deterioration of active materials. There is every possibility that discharge profiles change without

any variation of OCV. Therefore, the change of discharge profiles was investigated every week as well (Fig. 13). LFP showed significant changes in its profiles with a (not very serious) decrease of capacity and an increase of *IR* drop. On the contrary, there are no significant changes in the profiles of LMO. In terms of storage stability at 60 °C, therefore, LMO is superior to LFP, at least in the case of the additive-free electrolyte used in this study.

3.5 Cycle life

For HEV/EV applications, the long-term cyclability of battery cells should be guaranteed. The life of rechargeable batteries should not limit that of HEVs and EVs, when considering the cost of batteries and the replacement service fee. If low cost batteries are available, concern about the long-term stability could be reduced, and simultaneously the design to enable easy replacement of batteries should be devised.

To measure the cyclability of cells, the change of capacities with charge/discharge cycles were investigated at 20 °C (blue circles) and 60 °C (red circles) (Fig. 14). At room temperature, cells based on thinner electrodes for HEVs showed a smaller decrease of discharge capacity, compared with their thicker counterparts for EVs. Within the comparison group, in terms of application (HEVs or EVs), LMO is better than LFP. That is to say, the order of the performance of cyclability at room temperature is: LMO for HEVs > LMO for EVs, and LFP for HEVs > LFP for EVs.

At 60 °C, even if a more significant decrease of capacity with cycles was expected as a first guess, the cells for HEVs at 60 °C showed almost the same degree of cycle stability as the corresponding cells at room temperature. On the other hand, a very serious decrease was observed with EV cells based on thicker electrodes. The deterioration of cells at 60 °C would be caused by the dissolution of metal ions from LFP and LMO. These issues can be addressed by using proper additives in the electrolyte,[32] or by coating the active materials with an inert layer,[33] as mentioned above.

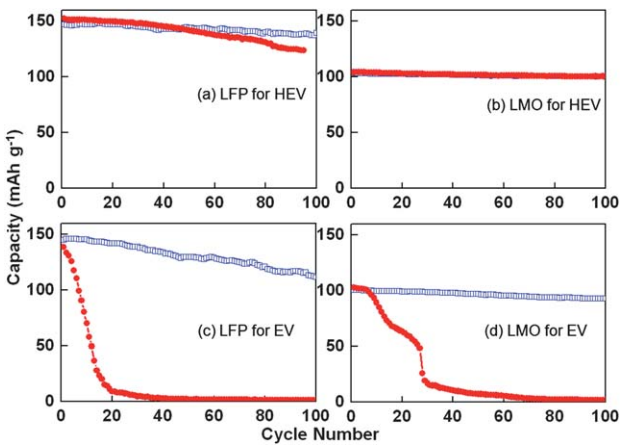

Fig. 14 Change of capacity with a cycle of charge and discharge at 20 °C (blue circles) and 60 °C (red circles). In each cycle, cells were charged to 4.3 V at 0.5 C, followed by keeping the potential constant until the current decreased to a hundredth of the initial current. Then, the cells were discharged at 1 C.

The dependency of cyclability on electrode thickness would be an interesting experimental result. Poor rate capability of thick electrodes is understandable because the dimension of the thickness represents the characteristic length of the ion/electron movement pathway, indicating resistance. High rate discharges lead to large *IR* drops. However, why the cycle life of cells depends on electrode thickness is unclear, even if the phenomenological facts were surely confirmed by at least five independent sets of experiments. This beyond the scope of this review article, and it is left for other works to reveal the exact reason for the dependency of cyclability on electrode thickness.

To support the half cell experiments, a full cell configuration was adopted with an anode (artificial graphite : PVdF = 92 : 8) (Fig. 15). Full HEV cells showed a more serious capacity decrease at 60 °C than that of their half cell counterparts: 30% and 20% decreases of capacity at the 50th cycle were observed with LFP and LMO, respectively, in the full cell configuration (note that no electrolyte additives were used to enhance cycling performance here).

In addition to the cyclability of cells at room temperature and high temperature, it should be considered how the cells work at low temperature. As expected, operation at temperatures below 0 °C leads to low capacity with a sustainable cyclability due to slow kinetics related to ion and/or electron transports in electrolyte, within electrode materials and at the interface between the electrode and electrolyte. The expected behavior at low temperatures has been reported for LFP,[34–36] while there are no articles for LMO as far as we know. At the same rate of discharge (0.1 C or 1 C), 80 to 85% of Q_{RT} (capacity at room temperature) was obtained at 0 °C for LFP; 65 to 70% of Q_{RT} at −20 °C; and 40 to 50% of Q_{RT} at −40 °C. The capacity decrease was attributed mainly to slow charge transfer at the interface between the electrode and electrolyte, and a slow diffusion of lithium ions in the electrode materials.[35] Charge transfer resistance (R_{CT}, ohm) increased 40 times and the diffusion coefficient (D, $cm^2\ s^{-1}$) decreased a hundredth at −40 °C when compared with those at

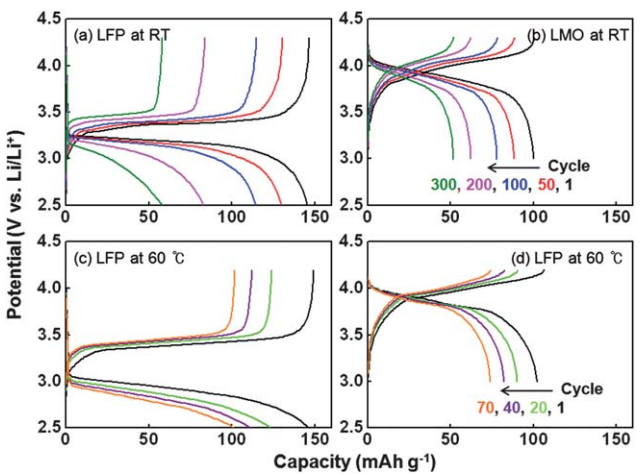

Fig. 15 Charge and discharge voltage profiles of LFP and LMO in full cells. The same electrode compositions for LFP and LMO were used as indicated in Fig. 11. Charge cut-off voltages for the cathodes were 4.3 V, but discharge cut-off voltages for LFP and LMO were 2.5 and 3 V, respectively. The cells were cycled at a 0.5 C rate under a constant current mode. The negative/positive ratio (N/P) was 1.06 for the Li-ion cell.

room temperature. The solution resistance (R_s, ohm) was not the governing factor. Cyclability was fairly sustainable without a particularly significant drop of capacity.[36]

4. Perspective: forward & toward

4.1 LMO

The power density (rate capability) of these cathode materials with bulk sizes is generally low due to the high level of polarization at high charge-discharge rates (above 2 C). In addition, electrode density should be considered as one of the factors affecting energy density: higher electrode density leads to higher energy density. This higher electrode density can be easily achieved by using large particles of the active materials. As a consequence, two benefits can be obtained by increasing the size of $LiMn_2O_4$ particles: high electrode density and low Mn dissolution. However, conversely, large particles can deteriorate the high rate capability (power). Hence, the best way to improve both rate capability and electrode density is to use bulk particles that consist of aggregated nano-sized particles. A wide variety of synthetic approaches for synthesizing $LiMn_2O_4$ nanoparticles (nanotubes, nanorods, nanowires and hollow morphologies) have been developed to improve the rate capabilities of spinel $LiMn_2O_4$ at room temperature.[37–44] However, these materials are quite bulky, and therefore their use is expected to entail a significant decrease in electrode density.

As discussed above, a disproportionation reaction starts on the particle surface, resulting in the formation of a defective spinel. The reaction moves progressively inward with increasing exposure to the electrolyte, especially at elevated temperatures. This reduces the intercalation capacity, and therefore should be prevented to ensure a long-cycle life for elevated-temperature performance. To reduce such inherent structural degradation, a marginal increase in the overall Mn valence to above +3.5 has been reported.[45–48] However, such methods do not significantly improve the structural stability since a fraction of Mn^{3+} ions still remain in the spinel structure. The most effective way to block Mn dissolution is to completely encapsulate the spinel particles with oxides that are resistant to acidic HF, and solution-based techniques, such as sol–gel, and solution precipitation, have been used for improving the high temperature cycling of the spinels.[49–54] However, these methods cannot lead to a uniform coating layer and can lead to difficulties in controlling the coating thickness as the coating precursors randomly adhere to the active materials during drying and annealing. Hence, coating with a uniform thickness is very difficult to control, and segregation of the coating is inevitable. If a metal oxide is uniformly coated on the spinels, capacity fade from the Mn dissolution should be significantly reduced, especially under extended cycling above 60 °C, which is a critical temperature for HEV application.

Fig. 16a shows a schematic diagram for the polyvinyl pyrrolidone (PVP)-functionalized metal oxide coating procedure. As-synthesized spinel nanoparticles were functionalized with PVP groups in distilled water.[55,56] Dissolved metal ions were then complexed with the entire PVP backbone, and the remaining ionic groups dissolved in water were removed by filtering. The filtered powder was heat-treated at 600 °C for 3 h in air. When the spinel nanoclusters were coated with same concentration of

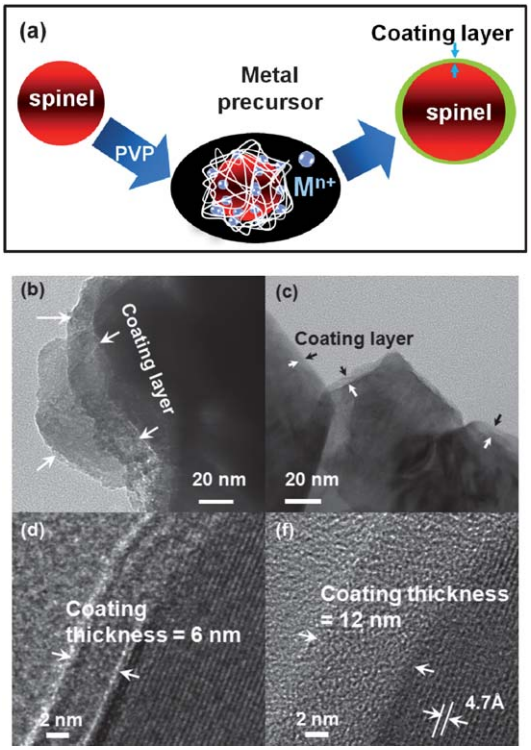

Fig. 16 (a) A schematic diagram for the PVP-functionalized metal oxide coating procedure, TEM images of ZrO_2-coated $LiMn_2O_4$ spinel cathodes (b) without using PVP, (c) with using PVP and with coating concentrations of (c) 1 wt% (image d is an expanded version of (c)) and (f) 2 wt%.

ZrC_2O_4 precursor without using PVP to coat the samples, the coating thickness was not uniform, and coating thickness varied from 10 to 100 nm (Fig. 16b). The coating thickness can be controlled by the amount of PVP used. When the amounts of metal oxide precursors were increased from 1 wt% to 2 wt%, the coating thickness increased from 6 nm (Fig. 16c and d) to 12 nm (Fig. 16f).

PVP-assisted ZrO_2 coating demonstrated significantly improved rate characteristics under cycling at 65 °C and exhibited over 60% improved capacity retention compared to the bare cathode, despite the high surface area.[55] The reason for this observed improvement was associated with the fact that the ZrO_2 coating layer minimized Mn dissolution from the spinel lattice.

4.2 LFP

With merits including low cost, low toxicity, high safety and good cycle stability, LFP has been developed in research and development to enhance its low electronic and ionic conductivity.[7,57,58] Strategies to overcome the demerits can be classified into four categories (Fig. 17): (i) enhancing the bulk properties in terms of electronic and ionic conductivity,[59–62] (ii) forming an Li^+-conductive surface layer,[63] (iii) forming an electron-conductive surface layer,[62,64] and (iv) reducing the characteristic length of particles.[1,65,66] Selected works are presented below as a representative for each strategy.

As the first strategy, Chung *et al.* solved the problem of low electronic conductivity of LFP by doping it with metals supervalent to Li^+ (M = Mg, Nb, Zr, and so on).[59] Solid-solution

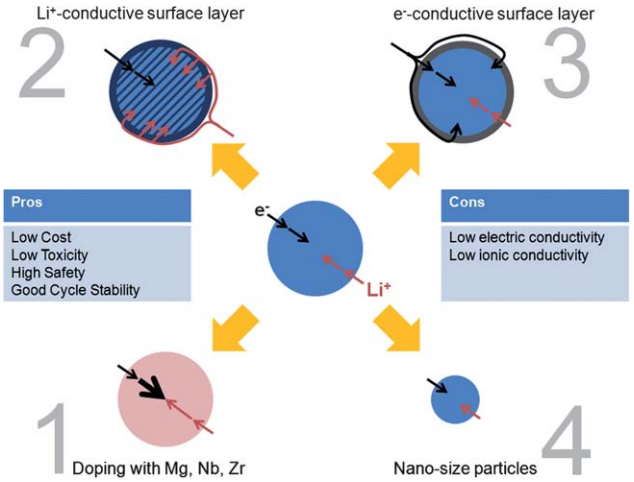

Fig. 17 Four strategies to enhance rate performance of LFP.

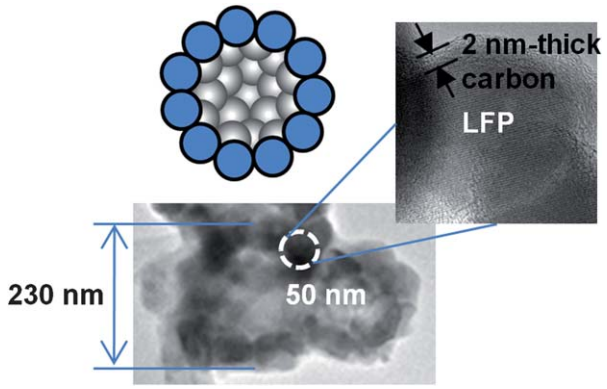

Fig. 18 A hollow sphere secondary structure of carbon-coated LFP nanoparticles.

doping was achieved by using a cationic non-stoichiometric (Li^+-deficient) synthesis, leading to $Li_{1-x}M_xFePO_4$. Conductivity tremendously increased from $10^{-9\ to\ -10}$ S cm^{-1} for an undoped LFP to 10^{-1-3} S cm^{-1} for doped ones. A weaker dependency of conductivity on temperature was investigated in doped LFP: $10^{-2\ to\ -1}$ S cm^{-1} at 25 to 300 °C for doped LFP *versus* $10^{-10\ to\ -6}$ S cm^{-1} for the undoped control. The high conductivity of bulk LFP led to a large capacity relative to its undoped control: 120 mA h g^{-1} at 1 C and 65 mA h g^{-1} at 20 C for doped LFP *versus* 25 mA h g^{-1} after 10 cycles at C/30.

As the second strategy, Kang and Ceder formed a fast ion-conducting surface phase on LFP by inducing off-stoichiometric compositions ($LiFe_{1-2y}P_{1-y}O_{4-\delta}$) specifically on the surface.[63] Li^+ travels *via* the surface phase $LiFe_{1-2y}P_{1-y}O_{4-\delta}$ before finding the [010] direction of core LFP through which Li ions diffuse. As they emphasized ultrafast charging as well as discharging in the title of this work, they showed very impressive fast discharging performances: 165 mA h g^{-1} at 2 C, 150 mA h g^{-1} at 10 C and 100 mA h g^{-1} at 50 C (measured from discharge from 4.3 V to 2.5 V with LFP : carbon : binder = 80 : 15 : 5). Moreover, >120 mA h g^{-1} was obtained at 200 C charge/discharge with a highly conductive electrode composition (LFP : carbon : binder = 30 : 65 : 5). Even if the composition includes an excessive amount of carbon as a conductivity enhancer, the meaning of 200 C is strikingly important: EVs can be charged within only 1/200 h = 18 s.

As the third strategy, conductive carbon coatings on LFP have been widely and extensively used to enhance electric conductivity of LFP particles.[64] Carbon precursors mixed with LFP or its precursors are converted into amorphous carbon during thermal treatment to develop olivine crystallinity. Herle *et al.* constructed a composite material system consisting of LFP, Fe_2P and C/$Fe_{75}P_{15}C_{10}$ *via* carbothermal chemistry.[62] The conductive nano-phase phosphide network was created following the grain boundaries of the insulating LFP nanocrystallites.

As the last strategy, the characteristic dimension of diffusion length and conductive pathway can be reduced by scaling down LFP particles from micrometer size to a nano-dimension.[1] Gaberscek *et al.* emphasized the nano-scaling rather than carbon coating because the ionic conductivity is lower than electronic one in LFP.

Even if the four strategies mentioned above are described separately, the improvement of material properties leading to enhanced performances results from synergetic combinations of the strategies. To obtain large capacities at high discharge rates, nanoparticles have been used with doping or an Li^+/e^--conductive layer coating. High dimensionalization or hierarchical structuring of nano-units would be a feasible direction of research and development, considering that all nanoparticles as the nano-units have been well evolved with accommodating and improved properties. Lee *et al.* showed the secondary structuring of primary particles of LFP is helpful for reducing *IR* drop especially during fast charge and discharge. A spherical nano-particle coated with carbon (diameter < 30 nm) was used as the primary particle. A hollow sphere (diameter = ~300 nm) was constructed with the primary nano-spheres in its shell (Fig. 18). The resultant structure showed a very small *IR* drop at high discharge rates: ΔIR(hollow) = 0.15 V at 10 C and 0.4 V at 50 C. The values of ΔIR for hollow-sphere-secondary-structured LFP are recognized as very small when compared with those of conventional non-hollow nanoparticles: ΔIR(non-hollow) = 0.95 V at 10 C and >1.45 V at 50 C. The small *IR* drop on discharge (that would originate from "easy accessibility of Li^+ to each primary particle caused by its hollow secondary structure") is analogous to the small *IR* rise during charge. The cells based on hollow LFP were charged up to 50 C (without potentiostatic charging) successfully, guaranteeing a significant amount of capacity on discharge: 120 mA h g^{-1} at 10 C and 100 mA h g^{-1} at 50 C.[67]

5. Conclusions

LFP and LMO were compared bibliographically and experimentally. Even if various strategies including bulk doping, electrically and ionically conductive coating and nono-dimensionalization have enabled the poor conductivities of LFP to be overcome, LMO still showed better discharge performances (especially rate capability) due to its superior intrinsic properties, compared with a practical grade of LFP (carbon-coated nano-particles). Moreover, the order relationship of gravimetric discharge capacity was reversed in terms of volumetric energy density, when the higher working potential and higher loading of

LMO in electrodes are considered: LFP > LMO in terms of Q_m^{dCh} to LFP < LMO in terms of ED_v^{dCh}.

On the other hand, LFP showed a better rate capability in terms of charge than LMO. This is not due to material properties but due to the operational conditions. When the cells are charged to 4.3 V, independent of materials, LMO has a very limited span of working potential during discharge, compared with LFP. Abrupt potential increase due to *IR* rise (contrary to *IR* drop) occurring during fast charging reaches the charging potential (4.3 V) so that cells cannot be charged.

By considering better the discharge performance of LMO and the faster charging capability of LFP, a proper cathode material could be selected depending on the required application. For example, in the event that a long time driving without plug-in is the essential criterion, LMO could be preferred. On the other hand, if fast charging was the main concern, LFP would have an advantage.

Even if both materials showed thermal stability, guaranteeing safety, the cyclability at high temperature (60 °C) should be enhanced. For HEVs (thinner electrodes), the capacity fading was not as serious as that of EVs. Both LFP and LMO showed very serious capacity decay in cells for EVs, probably due to metal dissolution. In a deviation from our first guess, LFP showed more problematic deterioration in cells. This problem can be overcome by using an additive or a proper surface coating on the cathode materials.

Acknowledgements

This work was supported by WCU/R31–2008-000–20012-0 and the Converging Research Center Program (2010K000984) through the National Research Foundation of Korea (NRF) funded by the Ministry of Education, Science and Technology.

References

1 M. Gaberscek, R. Dominko and J. Jamnik, *Electrochem. Commun.*, 2007, **9**, 2778.
2 J. Guan and M. L. Liu, *Solid State Ionics*, 1998, **110**, 21.
3 C. W. Wang, A. M. Sastry, K. A. Striebel and K. Zaghib, *J. Electrochem. Soc.*, 2005, **152**, A1001.
4 M. Tang, W. C. Carter and Y. M. Chiang, *Annu. Rev. Mater. Res.*, 2010, **40**, 501.
5 X. C. Tang, X. W. Song, P. Z. Shen and D. Z. Jia, *Electrochim. Acta*, 2005, **50**, 5581.
6 P. P. Prosini, M. Lisi, D. Zane and M. Pasquali, *Solid State Ionics*, 2002, **148**, 45.
7 D. Morgan, A. Van der Ven and G. Ceder, *Electrochem. Solid-State Lett.*, 2004, **7**, A30.
8 M. Yoshio, ed., *Lithium-Ion Batteries*, 2008, Springer, New York.
9 M. Yoshio, Y. Y. Xia, N. Kumada and S. H. Ma, *J. Power Sources*, 2001, **101**, 79.
10 M. M. Thackeray, *Prog. Solid State Chem.*, 1997, **25**, 1.
11 M. Wakihara, ed., *Lithium Ion Batteries: Fundamentals and Performance*, Wiley-VCH, Germany, 1998.
12 G.-A. Nazri, ed., *Lithium Batteries Science and Technology*, Wiley-VCH, Boston, 2004.
13 D. Aurbach and Y. Gofer, *J. Electrochem. Soc.*, 1991, **138**, 3529.
14 J. Cho, Y. J. Kim and B. Park, *Solid State Ionics*, 2001, **138**, 221.
15 R. J. Gummow, A. Dekock and M. M. Thackeray, *Solid State Ionics*, 1994, **69**, 59.
16 J. S. Gnanaraj, V. G. Pol, A. Gedanken and D. Aurbach, *Electrochem. Commun.*, 2003, **5**, 940.
17 A. Blyr, C. Sigala, G. Amatucci, D. Guyomard, Y. Chabre and J. M. Tarascon, *J. Electrochem. Soc.*, 1998, **145**, 194.
18 J. C. Hunter, *J. Solid State Chem.*, 1981, **39**, 142.
19 C. Sigala, D. Guyomard, A. Verbaere, Y. Piffard and M. Tournoux, *Solid State Ionics*, 1995, **81**, 167.
20 H. Kawai, M. Nagata, H. Kageyama, H. Tukamoto and A. R. West, *Electrochim. Acta*, 1999, **45**, 315.
21 H. Shigemura, H. Sakaebe, H. Kageyama, H. Kobayashi, A. R. West, R. Kanno, S. Morimoto, S. Nasu and M. Tabuchi, *J. Electrochem. Soc.*, 2001, **148**, A730.
22 M. Jo, Y. K. Lee, K. M. Kim and J. Cho, *J. Electrochem. Soc.*, 2010, **157**, A841.
23 M. M. Thackeray, A. Dekock, M. H. Rossouw, D. Liles, R. Bittihn and D. Hoge, *J. Electrochem. Soc.*, 1992, **139**, 363.
24 J. Cho and M. M. Thackeray, *J. Electrochem. Soc.*, 1999, **146**, 3577.
25 R. Benedek and M. M. Thackeray, *Electrochem. Solid-State Lett.*, 2006, **9**, A265.
26 J. Cho, *J. Mater. Chem.*, 2008, **18**, 2257.
27 F. T. Quinlan, K. Sano, T. Willey, R. Vidu, K. Tasaki and P. Stroeve, *Chem. Mater.*, 2001, **13**, 4207.
28 N. Iltchev, Y. K. Chen, S. Okada and J. Yamaki, *J. Power Sources*, 2003, **119**, 749.
29 M. Koltypin, D. Aurbach, L. Nazar and B. Ellis, *Electrochem. Solid-State Lett.*, 2007, **10**, A40.
30 K. Amine, J. Liu and I. Belharouak, *Electrochem. Commun.*, 2005, **7**, 669.
31 K. Amine, J. Liu, S. Kang, I. Belharouak, Y. Hyung, D. Vissers and G. Henriksen, *J. Power Sources*, 2004, **129**, 14.
32 H. C. Wu, C. Y. Su, D. T. Shieh, M. H. Yang and N. L. Wu, *Electrochem. Solid-State Lett.*, 2006, **9**, A537.
33 G. M. Song, Y. Wu, G. Liu and Q. Xu, *J. Alloys Compd.*, 2009, **487**, 214.
34 S. S. Zhang, K. Xu and T. R. Jow, *J. Power Sources*, 2006, **159**, 702.
35 X.-Z. Liao, Z.-F. Ma, Q. Gong, Y.-S. He, L. Pei and L.-J. Zeng, *Electrochem. Commun.*, 2008, **10**, 691.
36 X. D. Yan, G. L. Yang, J. Liu, Y. C. Ge, H. M. Xie, X. M. Pan and R. S. Wang, *Electrochim. Acta*, 2009, **54**, 5770.
37 X. X. Li, F. Y. Cheng, B. Guo and J. Chen, *J. Phys. Chem. B*, 2005, **109**, 14017.
38 L. Z. Zhang, J. C. Yu, A. W. Xu, Q. Li, K. W. Kwong and L. Wu, *Chem. Commun.*, 2003, 2910.
39 E. Hosono, T. Kudo, I. Honma, H. Matsuda and H. S. Zhou, *Nano Lett.*, 2009, **9**, 1045.
40 F. Jiao, J. L. Bao, A. H. Hill and P. G. Bruce, *Angew. Chem., Int. Ed.*, 2008, **47**, 9711.
41 J. Y. Luo, Y. G. Wang, H. M. Xiong and Y. Y. Xia, *Chem. Mater.*, 2007, **19**, 4791.
42 D. K. Kim, P. Muralidharan, H. W. Lee, R. Ruffo, Y. Yang, C. K. Chan, H. Peng, R. A. Huggins and Y. Cui, *Nano Lett.*, 2008, **8**, 3948.
43 J. Y. Luo and Y. Y. Xia, *Adv. Funct. Mater.*, 2007, **17**, 3877.
44 J. Y. Luo, L. Cheng and Y. Y. Xia, *Electrochem. Commun.*, 2007, **9**, 1404.
45 A. Antonini, C. Bellitto, M. Pasquali and G. Pistoia, *J. Electrochem. Soc.*, 1998, **145**, 2726.
46 Q. Feng, Y. Miyai, H. Kanoh and K. Ooi, *Langmuir*, 1992, **8**, 1861.
47 J. M. Han, S. T. Myung and Y. K. Sun, *J. Electrochem. Soc.*, 2006, **153**, A1290.
48 Y. K. Sun, C. S. Yoon, C. K. Kim, S. G. Youn, Y. S. Lee, M. Yoshio and I. H. Oh, *J. Mater. Chem.*, 2001, **11**, 2519.
49 Z. L. Liu, H. B. Wang, L. Fang, J. Y. Lee and L. M. Gan, *J. Power Sources*, 2002, **104**, 101.
50 Z. H. Zheng, Z. L. Tang, Z. T. Zhang, W. C. Shen and Y. H. Lin, *Solid State Ionics*, 2002, **148**, 317.
51 A. M. Kannan and A. Manthiram, *Electrochem. Solid-State Lett.*, 2002, **5**, A167.
52 J. Cho, G. B. Kim, H. S. Lim, C. S. Kim and S. I. Yoo, *Electrochem. Solid-State Lett.*, 1999, **2**, 607.
53 G. G. Amatucci, A. Blyr, C. Sigala, P. Alfonse and J. M. Tarascon, *Solid State Ionics*, 1997, **104**, 13.
54 J. P. Cho, T. J. Kim, Y. J. Kim and B. Park, *Chem. Commun.*, 2001, 1074.
55 S. Lim and J. Cho, *Electrochem. Commun.*, 2008, **10**, 1478.
56 S. Lim and J. Cho, *Chem. Commun.*, 2008, 4472.
57 M. S. Islam, D. J. Driscoll, C. A. J. Fisher and P. R. Slater, *Chem. Mater.*, 2005, **17**, 5085.
58 T. Maxisch, F. Zhou and G. Ceder, *Phys. Rev. B: Condens. Matter, Mater. Phys.*, 2006, **73**, 104301.

59 S. Y. Chung, J. T. Bloking and Y. M. Chiang, *Nat. Mater.*, 2002, **1**, 123.
60 S. Y. Chung and Y. M. Chiang, *Electrochem. Solid-State Lett.*, 2003, **6**, A278.
61 C. Delacourt, C. Wurm, L. Laffont, J. B. Leriche and C. Masquelier, *Solid State Ionics*, 2006, **177**, 333.
62 P. S. Herle, B. Ellis, N. Coombs and L. F. Nazar, *Nat. Mater.*, 2004, **3**, 147.
63 B. Kang and G. Ceder, *Nature*, 2009, **458**, 190.
64 N. Ravet, Y. Chouinard, J. F. Magnan, S. Besner, M. Gauthier and M. Armand, *J. Power Sources*, 2001, **97–8**, 503.
65 P. P. Prosini, M. Carewska, S. Scaccia, P. Wisniewski and M. Pasquali, *Electrochim. Acta*, 2003, **48**, 4205.
66 A. Singhal, G. Skandan, G. Amatucci, F. Badway, N. Ye, A. Manthiram, H. Ye and J. J. Xu, *J. Power Sources*, 2004, **129**, 38.
67 M. H. Lee, J. Y. Kim and H. K. Song, *Chem. Commun.*, 2010, **46**, 6795.